Validation of Simulated Mechanical Vibration Data for Operational State Recognition System

Jukka Junttila
VTT Technical Research Centre of Finland Ltd
Espoo, Finland
jukka.junttila@vtt.fi

Anssi Sillanpää
Wärtsilä Finland Oy
Vaasa, Finland
anssi.sillanpaa@wartsila.com

Ville Lämsä
VTT Technical Research Centre of Finland Ltd
Espoo, Finland
ville.s.lamsa@vtt.fi

Accurate real-time models for estimating the current state of an engine-generator set (genset) can be built based on measured mechanical vibration data. There is typically a significant disparity between the amount of data measured during normal and abnormal operation of a genset. Sufficient measured data to build a model for detecting and recognizing abnormal operation is rarely available. The lack of data measured during abnormal operation can be compensated, e.g., by creating more data through simulations. The focus of this study is on producing more realistic simulated vibration data by adding variations in the excitation forces used as input for the simulation. The added variations are based on the integration of previously measured cylinder pressure and rotational speed data from similar gensets as the simulated one. The effect of using varying input data on the simulated vibration responses of a genset is studied by extracting features and training operational state classifier models based on them. The extracted features and the classifier model results are compared with respect to the measured mechanical vibration data from a similar genset as the simulated one. The results show that the simulated responses resemble the measured ones. However, the comparative validation results reveal significant differences between the simulated and measured responses. Thus, further investigation and development is needed regarding production of the simulated mechanical vibration data.

Keywords—state estimation, classification, finite element method, simulation, mechanical vibration data, cylinder pressure

I. INTRODUCTION

Engine-generator sets (gensets) comprise a generator and an engine. Gensets are commonly used in remote or developing areas where, depending on the need, they can act as the primary or supplementary source of energy [1]. Another typical application for genset-based power plants is to serve as an emergency power supply in the event of a failure in the main power source [1].

Vast amounts of sensor-based measurement data are gathered from the gensets, and the extracted information is used to maximize and optimize the productivity of the machines [2]. Nevertheless, only little is known and implemented into usage regarding the data-based condition monitoring of the genset structures. The main premise is that the effective and efficient state recognition can be based on the extracted characteristics and features of the genset structures. Regarding the dynamic behavior of the genset structures, the extracted features are typically dynamic features such as natural mode shapes and the respective natural frequencies, signal statistics, or advanced physics-based indicators [3]. At the first level of condition monitoring [4], the discrete states of gensets could be presented as binary (intact/fault) or continuous (e.g., estimated power output level) variables. It is evident that the efficient state recognition procedures for genset structures require implemented and verified methods that are applicable for real-time operation [5].

Junttila [6] introduced methods for near real-time state recognition of the power output level and the transient abnormal operation of a Wärtsilä 20V31SG genset in his master's thesis. The presented methods were based on measured mechanical vibration data. The thesis proved that very accurate and fast classification of different power output levels of the studied genset is possible with machine learning (ML) models trained using traditional classifier algorithms such as support vector machines (SVM) or even linear regression (LR). The simple fact that elevating the power output increases the internal forces of an internal combustion engine (ICE), and the cyclic nature of the operation of an ICE at steady state, i.e., virtually constant rotational speed and virtually constant power output, were utilized when extracting the features for training the classifier models. This paper proposes a continuation of Junttila's master's thesis. It was proven in [6] that transient abnormal operation of a genset can be efficiently distinguished from normal operation based on the measured vibration response. Development of ML models capable for novelty detection [7], i.e., recognizing different types of abnormal operation of a genset, were identified as future work in [6]. However, the lack of labelled mechanical vibration data measured during abnormal operation of a genset stands in the way of training such models. A solution could be filling the shortage by simulated data.

The Wärtsilä 20V31SG engine is a four-stroke 20-cylinder turbocharged V-engine operating on spark-ignited gaseous fuel. The diameter of the cylinders is 31 cm. The 20V31SG genset is used in the electric power industry as the main component of engine power plants, typically there being more than one set in a single plant. For a 50 Hz utility frequency, the engine has a nominal rotational speed of 750 rpm with a maximum continuous power output of 11 MW. Marine applications for similar engines also exist [8].

Genset vibration simulations at Wärtsilä have typically been performed as steady-state analyses in frequency domain. Reference [9] contains an overview of the history of structural

978-1-6654-6603-5/22/$31.00 ©2022 IEEE
DOI 10.1109/IRI54793.2022.00040

dynamic simulation at Wärtsilä from the perspective of engine research and development, with a substantial number of further references. The excitation forces used as input for the typical genset vibration simulations have been defined assuming constant engine rotational speed and constant engine loading. In other words, the cylinder pressure curve used for calculating the excitation forces at a specific power output level is invariant between all the cylinders of the engine and between all the engine cycles. In a linear system, such as the studied one, this obviously leads to the simulated responses reaching and maintaining a vibrationally steady state and consequently to a trivial classification problem as each simulated power output level has an individual and invariant vibration response.

Therefore, the focus of this study was on developing the methods for calculating the excitation forces used as input for the vibration simulations to be able to produce more realistic simulated mechanical vibration response data than previously. To validate the simulated data produced in this study it was compared with corresponding measured data. The validation was done using data representing the normal operation of the genset as it was the only kind of labelled data available. In this study, normal operation of the genset refers to the state of virtually constant power output at virtually constant engine rotational speed over a period of at least some minutes. The different states or classes of normal operation of the genset refer to different levels of constant power output, which can be expressed for example as a percentage of the rated power of the genset.

The objective of the study was therefore to produce realistic simulated mechanical vibration response data of the different states of normal operation of the genset and validate the simulated data by comparing it to corresponding measured data. To reach the goals, variations were introduced in the engine rotational speed and in the cylinder pressure curves used for calculating the excitation forces used as input for the simulation. The variations are based on measured engine rotational speed and cylinder pressure histories, and thus, an essential part of the simulation input data is an integration of reused measured cylinder pressure and rotational speed data.

The methods used for defining the input, as well as the simulation model and analysis type are described more thoroughly in the following chapter. The next chapter also includes a short description of the feature extraction and normal operational state classification processes used in this study. The third chapter contains the results of the comparisons between the extracted features from the measured and simulated mechanical vibration data as well as the results of the comparisons between the operational state classification models built based on the extracted features. The results are discussed in detail in the fourth chapter which is followed by the conclusions presented in the fifth chapter.

II. Methods

This chapter presents the definition of the input, as well as the simulation model and analysis type. Finally, a short description of the feature extraction and normal operational state recognition processes are given.

A. Finite element analyses and model

The finite element (FE) simulation model of the genset shown in Fig. 1 contains an engine, a generator, and a base frame which have been geometrically discretized primarily into tetrahedral elements. The discretized engine has been condensed into a superelement (substructure) to reduce computational cost, with only visualization elements shown. The genset model utilizing the superelement has approximately 14 million degrees of freedom. The mass and length of the model are approximately 180 000 kg and 15 m, respectively. The model has agreed well with measured natural vibration frequencies. Simulated vibration velocities during engine operation evaluated at standardized locations on the genset have agreed sufficiently with measurements, with occasional significant differences. Modifying the existing FE model was not in the scope of the work. The simulation software was Abaqus by Dassault Systèmes.

The mechanical loading in a genset vibration simulation is the excitation forces caused by the operation of the engine. Typically, the excitation forces are applied to the cylinder heads, the cylinder liners, and the main bearings of the engine, and they consist of the gas forces caused by the cylinder pressure and of the mass forces accounting for the inertia of the slider-crank mechanism, which is not physically moving in the simulation to reduce computational cost.

Factors affecting the excitation forces are e.g., the cylinder pressure over the two-revolution four-stroke cycle as a function of crank angle (cylinder pressure curve), dimensions and inertia properties of the slider-crank mechanism components (pistons, connecting rods, crankshaft, etc.), cylinder firing order, V-angle, and rotational speed. The elasticity of the components, most notably the bending and torsional deflections of the crankshaft, is not considered in the excitation definition. The Python programming language was used to generate the excitations.

Genset steady-state vibration simulations at Wärtsilä have typically been performed in frequency domain, with a common cylinder pressure curve for all cylinders and with a constant rotational speed. Here the simulations were performed in time domain with variable cylinder pressure curves and variable rotational speed. As in frequency-domain cases, the simulations were linear and utilized superposition of natural vibration modes. The excitation forces for this study were defined based on engine rotational speed and cylinder pressure curves measured during normal operation. Measured cylinder pressure curves were available at power levels 100%, 85%, and 75% of

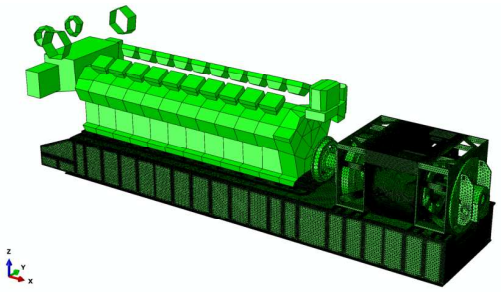

Fig. 1: FE simulation model of the genset, with the engine as a superelement.

the rated power. The excitation forces were defined for the aforesaid power levels.

Analyzing the measured engine rotational speed histories shows that they contain, as expected, Fourier components at the multiples of the engine cycle frequency (high-frequency content) and at significantly lower frequencies (low-frequency content). The former is assumed to be principally caused by local torsional deflection of the crankshaft at the measurement location and therefore not significant considering the rotational speed of the complete shaft line of the genset. The lengths of the signals, mean values and the standard deviations (SDs) of the measured rotational speed histories of the studied genset at different power output levels as well as the SDs of the measured rotational speed histories after removing all frequency components over 3 Hz are presented in Table I.

For each analyzed power level (100%, 85%, 75%), a synthetic rotational speed history with a duration of 240 s and a time step of 1/2048 s was created using the measured rotational speed data as a reference. Only the low-frequency content of the measured rotational speed was considered. The synthetic histories are visualized in Fig. 2 and the measured ones in Fig. 3. Since the low-frequency content had too low frequencies to be extracted by available fast Fourier transform (FFT) tools, engineering judgement was utilized by choosing appropriate low-frequency sinusoids, with the most dominant one having a frequency of 1/60 Hz, to create histories that sufficiently resembled the trend curve of the measured rotational speed. The trend curve of the rotational speed in a steady state is constant in principle but non-constant in practice due to fluctuations that are common in the operation of an ICE. The synthetic rotational speed histories had the same set of frequencies and amplitudes but different phases.

To estimate the variation of cylinder pressure curves between cycles, the relative standard deviation of peak cylinder pressure (4.2%) was extracted from an available cylinder pressure history measured from one cylinder of a different Wärtsilä engine. Reference [10] summarizes the essentials on cylinder pressure fluctuations and the forces acting on the ICEs.

Each synthetic rotational speed history was differentiated with respect to time and then scaled such that the mean was equal to unity and the standard deviation equal to the measured relative standard deviation of peak cylinder pressure. The resulting global scaling factor history for cylinder pressure approximated the dependency between rotational acceleration and combined cylinder pressure over all cylinders. The history was divided into engine cycles, and for each two consecutive cycles (four revolutions) the mean scaling factor value was determined.

Additional local cylinder-specific scaling factors for cylinder pressure were created for each engine cycle by randomly sampling a normal distribution having a mean of unity and a standard deviation equal to the measured relative standard deviation of peak cylinder pressure. Furthermore, the sample mean was made equal to unity for each engine cycle. The purpose of the local scaling factors was to ensure that the cylinder pressure curve in the simulations varied not only between engine cycles, but also between cylinders within an engine cycle.

TABLE I. MEASURED ROTATIONAL SPEED HISTORIES

Data properties	Power output level (%)			
	50	***90***	***95***	***100***
Length (min)	42	28	85	96
Mean (rpm)	749.74	749.89	750.13	750.09
SD (rpm)	1.79	2.66	2.82	2.93
SD filtered (rpm)	0.48	0.62	0.66	0.47

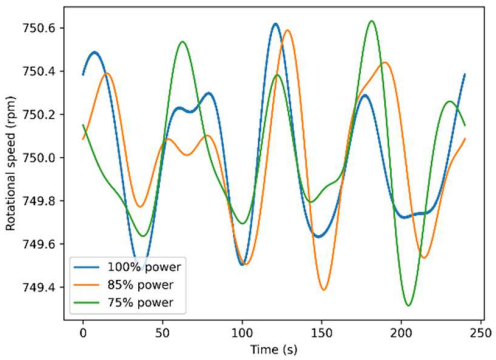

Fig. 2: Synthetic rotational speed histories. Updated, i.e., including the low-amplitude high-frequency components (not visible at this scale).

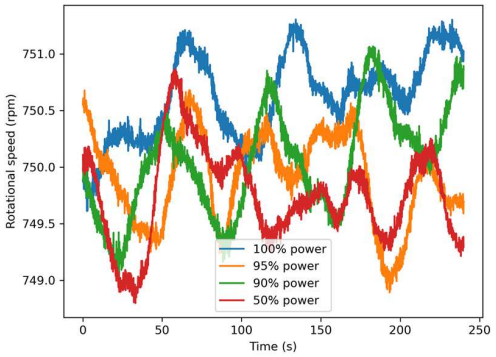

Fig. 3: Measured rotational speed histories.

An averaged measured cylinder pressure curve typically used in a frequency-domain simulation was used as a reference curve for all cylinders, with one reference curve per power level. The scaling of the reference cylinder pressure curve was performed using a modified Tukey window, with which scaling equal to the value of the scaling factor occurred near the peak cylinder pressure and scaling of unity occurred near the low-pressure areas of the curve, with a smooth transition in between. This is visualized in Fig. 4.

The scaling factor for a cylinder cycle was determined by multiplying the current two-cycle mean of the global scaling factor with the current local cylinder-specific scaling factor. The current values for these two factors were the values at that engine cycle which was ongoing when the peak pressure for the examined cylinder occurred at the examined cylinder cycle. Here the difference between an engine cycle and a cylinder cycle is that the first engine cycle started from the beginning of the analysis, but the starting point of a cylinder cycle was the beginning of its intake stroke. The starting points of cylinder

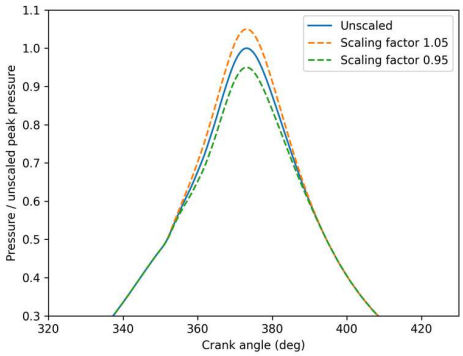

Fig. 4: Example of the scaling of the reference cylinder pressure curve (100% power) using a modified Tukey window. The cycle starts at 0 degrees and ends at 720 degrees.

cycles varied per cylinder since the cylinders generally do not operate in the same phase.

For each power level, the engine torque history was calculated with the excitation force Python script using the synthetic rotational speed history and the cylinder pressure scaling factor histories. The engine torque history was then integrated with respect to time and scaled to sufficiently match the original synthetic rotational speed history. The result was effectively the rotational speed history but including high-frequency components. However, there was only one such component present (and its multiples, but with very low amplitudes) due to the characteristics of the engine balance and since the crankshaft was idealized as infinitely rigid in the excitation definition. This component was the firing frequency (here five times the rotational frequency) and its amplitude was small relative to the low-frequency content. For better conformance with the original synthetic rotational speed history, the high-frequency component and some of its lowest multiples were isolated using a Butterworth filter and then added to the original synthetic rotational speed history.

The final excitation forces were created using the excitation force Python script again with the updated synthetic rotational speed histories. The forces were written into text files in a format supported by the FE simulation software. The vibration simulations of the genset were executed by first extracting an appropriate number of natural vibration modes, after which a mode-based forced vibration analysis in time domain was performed for each engine power level. The excitation forces and the time-domain analyses had the same time step as the synthetic rotational speed histories. Vibration acceleration data from 57 measurement points of interest were extracted from the simulation result files using a Python script.

B. Feature extraction and operational state recognition models

The operational state recognition process for the studied genset using mechanical vibration data has been described in detail in [6]. Only the most important parts of the process considering this study are presented in this chapter. As mentioned in the introduction the classification of different power output levels of the studied genset can be done very accurately in near real-time using ML models. Classifiers trained using the SVM algorithm gave the most accurate predictions but were significantly slower in predicting compared to classifiers trained using other algorithms. In [6] the LR algorithm was proven to be very efficient for training both accurate and fast-predicting classifiers and was therefore used for building the operational state recognition models of this study.

Two different functions were used for the feature extraction from the simulated mechanical vibration data. The models trained using the feature values extracted with the two functions gave the most accurate classification results according to [6]. The first of the feature extraction functions was used to calculate the signal power (feature name: PWR) and the second was used to calculate the peak vibration amplitude at the frequency equivalent to 1.5 times the rotational frequency of the engine (feature name: RF15).

The feature values were extracted from short signal segments of lengths from one to seven multiples of the length of an engine cycle. At 750 rpm, i.e., the rated rotational speed of the studied genset, one engine cycle (four-stroke cycle) takes 0.16 seconds. Using shorter signal segment gives predictions that are closer to real-time but on the other hand, the prediction accuracy is lower due to greater sensibility to the fluctuations in the operation of the engine.

Feature values were defined for the 57 examined measurement points of interest. The two feature extraction functions were applied separately for the simulated mechanical vibration histories in the three cartesian directions and using the seven different signal segment lengths. Therefore, 42 (two functions × three cartesian directions × seven segment lengths) different feature values were defined for each measurement point. Operational state recognition models were built separately for each point and for each of the seven segment lengths to classify the three analyzed power levels (100%, 85%, 75%). The features extracted using the two feature extraction functions were used to train the operational state recognition models both separately and combined, i.e., three different feature selections (PWR, RF15, both). In total 1197 models (57 measurement points × seven segment lengths × three feature selections) were built.

Measured data was available only from four different locations (P1, P2, P3, and P4). The measurement points P1, P3, and P4 were located on different parts of the generator and the measurement point P2 on the base frame under the generator. Therefore, the validation of the simulated mechanical vibration data was done by comparing them with the corresponding measured data from the four points. Measured data was available from the following six levels of power output of the rated power of the genset: 100%, 95%, 90%, 75%, 50%, and 0%.

III. RESULTS

The comparative validation results between the measured (M) and the simulated (S) cases are presented in the following chapters. The comparative results for the extracted features and the classification results of the state recognition by the LR classifiers are presented separately.

A. Extracted features

The comparative validation results of the extracted features, i.e., scaled means and relative percentual standard deviations of the feature values, are presented in Tables II, III, and IV. Before presenting the extracted feature values they were scaled so that the mean for each feature for the 100% power output equals one. Therefore, only the mean feature values for the 75% power output are presented.

TABLE II. MEANS OF THE PWR FEATURE VALUES AT 75% LOAD

Co-ordinate	Measurement point							
	P1		*P2*		*P3*		*P4*	
	M	*S*	*M*	*S*	*M*	*S*	*M*	*S*
X	0.61	0.59	0.59	0.57	0.35	0.58	0.27	0.58
Y	0.62	0.57	0.63	0.57	0.77	0.57	0.87	0.56
Z	0.64	0.60	0.64	0.57	0.56	0.58	0.32	0.60

TABLE III. MEANS OF THE RF15 FEATURE VALUES AT 75% LOAD

Co-ordinate	Measurement point							
	P1		*P2*		*P3*		*P4*	
	M	*S*	*M*	*S*	*M*	*S*	*M*	*S*
X	0.80	0.77	0.74	0.78	0.51	0.77	0.47	0.77
Y	0.68	0.77	0.78	0.76	0.76	0.77	0.76	0.77
Z	0.62	0.77	0.87	0.77	0.57	0.77	0.60	0.77

TABLE IV. RELATIVE STANDARD DEVIATIONS (%) OF THE FEATURES

Signal length (cycle)	Feature and power output level (%)							
	PWR 75		*PWR 100*		*RF15 75*		*RF15 100*	
	M	*S*	*M*	*S*	*M*	*S*	*M*	*S*
1	5.8	5.9	13.6	10.5	6.6	3.4	12.1	4.4
2	4.8	5.8	6.2	10.4	5.2	2.3	6.2	3.0
3	4.6	5.8	7.2	10.4	4.8	1.7	6.7	2.2
4	4.5	5.8	5.5	10.4	4.6	1.6	5.3	2.0
5	4.4	5.8	6.1	10.3	4.4	1.5	5.6	1.9
6	4.4	5.8	5.3	10.3	4.3	1.4	5.0	1.8
7	4.3	5.8	5.6	10.3	4.2	1.4	5.2	1.7

B. State recognition

The comparative validation results of the state recognition in the four validation locations for the different signal lengths are presented in Tables V, VI, and VII. Tables V and VI present the classification accuracies of the state recognition models trained using the PWR and RF15 features, respectively. In Table VII, the obtained results are produced by using both features. Table VIII presents the number of perfect classifiers individually for the seven different signal lengths and for the three different feature selections out of a possible 57.

TABLE V. ACCURACIES (%) OF CLASSIFIERS USING PWR FEATURE

Signal length (cycle)	Measurement point							
	P1		*P2*		*P3*		*P4*	
	M	*S*	*M*	*S*	*M*	*S*	*M*	*S*
1	91.4	82.0	78.8	99.0	93.5	92.3	68.7	90.0
2	93.4	84.7	83.5	99.8	96.1	95.5	76.3	91.9
3	94.0	86.5	85.4	99.9	96.8	97.2	79.4	92.7
4	94.5	87.8	86.5	100	97.4	98.4	81.2	93.4
5	94.7	88.7	87.1	100	97.7	99.0	82.2	94.2
6	94.9	89.4	87.7	100	98.0	99.3	82.9	94.9
7	95.1	89.9	88.1	100	98.1	99.5	83.5	95.8

TABLE VI. ACCURACIES (%) OF CLASSIFIERS USING RF15 FEATURE

Signal length (cycle)	Measurement point							
	P1		*P2*		*P3*		*P4*	
	M	*S*	*M*	*S*	*M*	*S*	*M*	*S*
1	88.1	99.2	91.1	100	75.9	81.6	95.3	100
2	94.9	99.9	96.2	100	88.5	92.9	96.1	100
3	91.3	100	94.5	100	82.2	97.7	91.7	100
4	95.7	100	97.2	100	91.4	97.9	97.1	100
5	93.3	100	95.8	100	86.3	98.3	94.8	100
6	96.0	100	97.8	100	92.5	98.9	97.5	100
7	94.6	100	96.4	100	88.9	98.8	96.3	100

TABLE VII. ACCURACIES (%) OF CLASSIFIERS USING BOTH FEATURES

Signal length (cycle)	Measurement point							
	P1		*P2*		*P3*		*P4*	
	M	*S*	*M*	*S*	*M*	*S*	*M*	*S*
1	95.1	99.2	92.2	100	95.1	81.6	87.8	100
2	98.7	99.9	96.7	100	97.7	92.9	97.4	100
3	97.8	100	95.5	100	97.7	97.7	93.6	100
4	99.5	100	97.9	100	98.9	97.9	98.6	100
5	98.8	100	96.6	100	98.5	98.3	96.3	100
6	99.7	100	98.5	100	99.2	98.9	99.1	100
7	99.2	100	97.3	100	98.9	98.8	97.7	100

TABLE VIII. NUMBER OF PERFECT CLASSIFIER MODELS

Feature	Signal length (cycle)						
	1	*2*	*3*	*4*	*5*	*6*	*7*
PWR	1	3	4	9	12	15	14
RF15	5	32	42	48	49	50	52
Both	5	32	42	48	49	50	52

IV. Discussion

When comparing the accuracies of the state recognition models it must be taken into consideration that the models built using the measured data classify between six classes (100%, 95%, 90%, 75%, 50%, and 0%), whilst the models built using the simulated data classify between three classes (100%, 85%, and 75%). Most of the incorrect predictions by the models built using the measured data were made between the first three classes [6]. Therefore, it was expected that the accuracies of the models built using the measured data are somewhat lower than the models built using the simulated data.

According to the results shown in the previous chapter there is enough variation in the simulated data so that only just over half of the trained operational state recognition models (614 of 1197) are perfect classifiers. Analysis of the classification results by measurement point demonstrates that the most accurate classifiers were achieved using the simulated feature values extracted from the points P2 and P4. The result is contrary compared to the corresponding classifier accuracies achieved using the measured feature values where the most accurate models were achieved using feature values extracted from the data measured from points P1 and P3. There is no apparent reason to expect that corresponding comparative validation results obtained using other classifier algorithms, such as those in [6], would be significantly different.

When comparing the simulated and measured feature values and the classifying accuracies of the state recognition models trained using them, the variation in the simulated feature values extracted using the PWR function is slightly higher than in the corresponding measured values. Considering the feature values extracted using the RF15 function the relation between the simulated and measured values is reverse and the differences between them are more notable. In fact, the variance in the simulated RF15 feature values is so low that using the values of both feature values for building the state recognition models instead of only the RF15 feature values does not increase the number of perfect classifiers. There is not as notable a difference between the feature values extracted from one and two cycles long segments of the simulated signals as there is between the feature values extracted from the corresponding measured signal segments.

The comparison of the mean feature values extracted from the simulated and measured data shows that generally they correspond well with each other. However, there is very little difference between the magnitudes of the mean feature values extracted from the simulated data in the different directions (X, Y, and Z) for a specific point, whereas between the corresponding feature values extracted from the measured data the differences are significant, especially considering feature values related to points P3 and P4.

V. Conclusions

Reuse and integration of previously measured data was successfully implemented in introducing variations in the definition of the excitation forces used as the input for the simulations. As expected, adding variation to the excitation forces leads to varying simulated vibration responses. Thus, the simulated responses resemble the measured ones. Moreover, the accuracy of state recognition models based on the simulated data is very high overall but not perfect in all cases, which is also in accordance with the expectations. However, the comparative validation results reveal significant differences between the simulated and measured responses. The obtained results indicate that the variation in the frequency content of the simulated responses is notably different from the measured. Therefore, the frequency content of the excitation forces and of their sources, especially of the cylinder pressure curve should be studied. The variation of the cylinder pressure was significantly greater than the variation of the rotational speed, and thus the effect of the former to the generated excitation forces was undoubtedly more dominant. It should also be noted that physically the rotational speed and the cylinder pressure are strongly coupled even though in the excitation generation these quantities were treated as more separate.

The measurement points used for the validation are located far from the excitation sources. The simulation method used does not consider the effect of possible nonlinearities, such as joints, that exist between the measurement point and excitation locations. Therefore, if available, mechanical vibration data measured from the engine, i.e., closer to the excitation sources, should be used in the validation as well. Additionally, the underlaying FE model could be revised. Thus, further investigation is needed regarding the simulation of the excitation forces, the simulation of responses, and the state recognition. Once the state recognition system is validated with the vibration data representing the normal operational state, the next obvious task is to compensate the lack of measured data of abnormal operation by simulations. Thus, the novelty detection approach will be investigated and implemented thoroughly.

References

[1] P. Breeze, Piston Engine-Based Power Plants, Academic Press, 2018.

[2] G. Pirker and A. Wimmer, “Sustainable power generation with large gas engines,” Energy Conversion and Management, vol. 149, pp. 1048–1065, 2017.

[3] W. Caesarendra and T. Tjahjowidodo, “A review of feature extraction methods in vibration-based condition monitoring and its application for degradation trend estimation of low-speed slew bearing,” Machines, vol. 5, no. 4, p. 21, Sep. 2017.

[4] K. Worden, C. R. Farrar, G. Manson, and G. Park, “The fundamental axioms of structural health monitoring,” Proceedings of the Royal Society A: Mathematical, Physical and Engineering Sciences, vol. 463, pp. 1639–1664, June 2007.

[5] P. K. Wong, Z. Yang, C. M. Vong, and Jianhua Zhong, “Real-time fault diagnosis for gas turbine generator systems using extreme learning machine,” Neurocomputing, vol. 128, pp. 249–257, March 2014.

[6] J. Junttila, Operational State Recognition of a Rotating Machine Based on Measured Mechanical Vibration Data, M. thesis, Arcada University of Applied Sciences, June 2021.

[7] M. Markou and S. Singh, “Novelty detection: a review—part 1: statistical approaches,” Signal Processing, vol. 83, no. 12, pp. 2481–2497, Dec. 2003.

[8] U. Åstrand, “Modular medium speed four-stroke engine,” MTZ industrial, vol. 6, no. 3, pp. 14–21, Aug. 2016.

[9] T. Frondelius, H. Tienhaara, and M. Haataja, ”History of structural analysis & dynamics of Wärtsilä medium speed engines,” Rakenteiden Mekaniikka, vol. 51, no. 2, pp. 1–31, Dec. 2018.

[10] R. Van Basshuysen and F. Schäfer, Internal Combustion Engine Handbook - Basics, Components, System, and Perspectives, 2nd edition, SAE International, 2016.